WILEY-VCH

Advanced Materials, 2019, 1904387

"Lattice strain matching" enabled nanocomposite design to harness the exceptional mechanical properties of nanomaterials in bulk forms

Junsong Zhang, Yinong Liu, Lishan Cui*, Shijie Hao, Daqiang Jiang, Kaiyuan Yu, Shengcheng Mao, Yang Ren, and Hong Yang*

Dr. J. Zhang, Prof. Y. Liu, Prof. H. Yang
Department of Mechanical Engineering, The University of Western Australia, Perth, WA 6009, Australia
E-mail: yinong.liu@uwa.edu.au

Prof. L. Cui, Prof. S. Hao, Dr. D. Jiang, Dr. K. Yu
Department of Materials Science and Engineering, China University of Petroleum-Beijing, Changping, Beijing 102249, China
E-mail: lscui@cup.edu.cn

Prof. S. Mao
Beijing Key Laboratory of Microstructure and Property of Advanced Materials, Beijing University of Technology, 100124 Beijing, China

Dr. Y. Ren
X-ray Science Division, Argonne National Laboratory, Argonne, IL 60439, USA

Keywords: nanocomposite, martensitic transformation, shape memory alloy, theoretical strength, elastic strain

Abstract

Nano-sized materials are known to have the ability to withstand ultra-large elastic strains (4~10%) and ultra-high strengths approaching their theoretical limits. However, it has been a long-standing challenge to harnessing their exceptional intrinsic mechanical properties in bulk forms. This has been commonly known as "the valley of death" in nanocomposite design. In 2013 we made a breakthrough to overcome this challenge by using a martensitic phase transforming matrix to create a composite in which ultra-large elastic lattice strains up to 6.7% were achieved in Nb nanoribbons embedded in it. This breakthrough was enabled by a novel concept of phase transformation assisted lattice strain matching between the uniform ultra-large elastic strains (4~10%) of nanomaterials and the uniform crystallographic lattice distortion strains (4~10%) of the martensitic phase transformation of the matrix. This novel concept has opened new opportunities for developing materials of exceptional mechanical properties or enhanced functional properties that had not been possible before. This paper reports on our work in progress in this research in the past 6 years.

1. Introduction – the challenge

Materials in nanodimensions are known to exhibit extraordinary mechanical properties, including ultra-high strengths to the order of tens of gigapascals and ultra large elastic strains to the order of over 10%.[1-9] For example, nanoscale diamond needles have been measured to exhibit a large elastic strain of 9%, which corresponds to a strength of ~98 GPa.[4] Yue et al.

deformed single crystal Cu nanowires in-situ under high resolution transmission electron microscope and observed a large elastic strain of 7.2%.[5] Wang et al. studied the fracture strength of Al_2O_3 nanowires by bending them to rupture and determined an elastic strain of 8.5% and a corresponding fracture strength of 39 GPa.[6] The origin of such extraordinary properties resides in the interatomic bonds within the solids. Such properties are approaching the theoretical limits expected based on $\sigma_{ideal} \approx 0.1E$ and predicted in more recent years by molecular dynamic and *ab initio* calculations.[10-12]

However, due to their extremely small sizes, nanomaterials cannot be used in large scale, particularly as loading-bearing materials in engineering applications. For this it has long been a desire to develop bulk composites incorporating these nanomaterials to harness their extraordinary properties in bulk applicable materials.[13] However, little success has been achieved.[13] The elastic strains (thus strength contributions) of the nanomaterials embedded in the composites have been generally below 1.0%, which is much lower than the intrinsic abilities as demonstrated by the corresponding freestanding nanomaterials.

The lack of success has been generally attributed to the imperfections in microstructure of the composites, including poor shapes and sizes of the nanomaterials embedded in, non-ideal alignment and distribution of the nanoinclusion, and poor bonding at the interfaces between the nanoinclusion and the matrix.[13,14] Encouraged by this understanding, much effort has been given in the past to design and process nanocomposite with improved microstructures to overcome these limitations. A best success may be represented by a Cu matrix – Nb nanowire composite.[15,16] In this composite, the Nb nanowires are perfectly aligned, well-dispersed, have high length-to-diameter aspect ratios, and have clean interface and strong bonding with the matrix. Despite these, the highest elastic latutce strains achieved in the Nb nanowires is still below 1.5%.[15,16] This is still far below the large elastic strains expected of the many freestanding nano-sized materials.[1-9]

Reflecting on the many failed attempts in carbon nanotube in polymeric matrix composite systems, Dzenis commented in *Science* in 2008 that “intensive work is under way, but the prospect of bulk structural super-nanocomposites appears more remote now than it did just a few years ago” and that “it is not even clear whether such translation is possible”.[13] These comments reflect very close to the general situation of all nanoinclusion composites, and it has commonly been regarded “the valley of death” for bulk nanocomposite materials design.

2. The Concept

We proposed a new concept in 2013.[17] It is based on an understanding of the mechanism of deformation in metals at the lattice level. In a plastically deforming metal matrix, a dislocation causes 100% local lattice stain whereas the rest of the matrix experiences elastic deformation typically to the order of <0.3% strain. In comparison, a nanowire embedded in the matrix is expected to deform elastically, up to ~7%, and the elastic strain is uniform at the lattice level. This implies a lattice strain mismatch between the nanowires and the matrix. This situation is expressed in **Figure 1**(a). The illustration depicts a hypothetical situation in which a nanowire-metal matrix composite (i) is deformed to 3% global strain (ii). In the plastically deforming matrix, this global strain is (hypothetically) realized by the formation of three dislocations within every 100 crystallographic planes, each causing 100% local strain within the lattice whereas the rest of the lattice away from the dislocations deforms elastically to a nominal 0.2% lattice stain, as expressed by the blue curve. In comparison, the embedded nanowires, if standing free, would deform uniformly to 3% elastic strain, as expressed by the red curve. There is clearly a mismatch between the uniform elastic strain of the nanowires and the heterogeneous

lattice stains in the plastically deforming matrix, particularly the highly localized lattice strain concentrations at the dislocations and the very low lattice stains elsewhere. This mismatch jeopardizes effective load transfer from the matrix to the nanowires, thus the chance to induce large elastic strains in them. This explains the reason of the failures of the nanowire composites in the past decades.

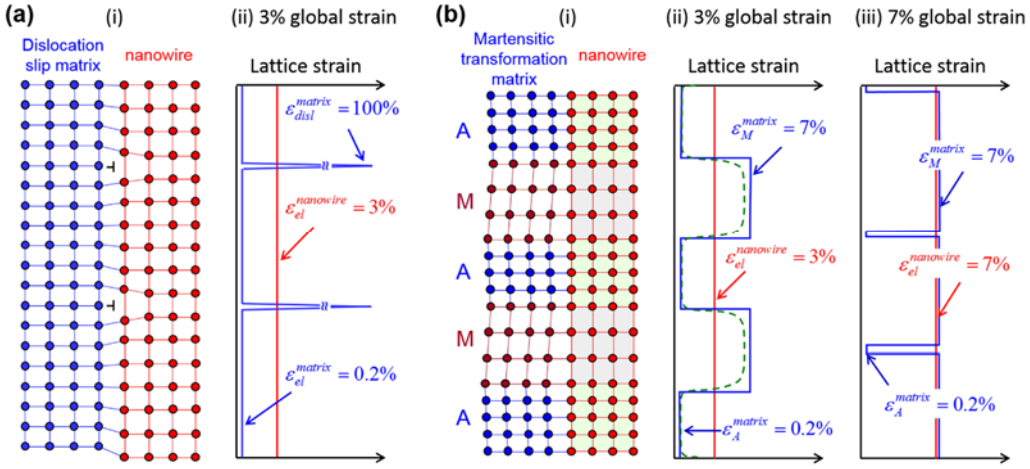

Figure 1. Schematic illustration of the concept of martensitic transformation assisted "lattice strain matching" for nanowire composites. (a) Lattice strain mismatch between a plastically deforming matrix and a nanowire in a composite. (b) Lattice strain matching between a martensitic transforming matrix and a nanowire in a composite.

The new concept utilizes thermoelastic martensitic transformation in a matrix, for example the B2-B19' martensitic transformation in NiTi shape memory alloy. This transformation is associated with a lattice strain of ~7%. This situation is illustrated in Figure 1(b). Upon a global deformation of 3% strain to the composite, the NiTi matrix will deform via a partial B2→B19' martensitic transformation, as depicted in (i). In this case the matrix will have a proportionally distributed regions of two different lattice strains, corresponding to the elastic deformation of the B2 austenite (A) at 0.2% strain and the stress-induced B19' martensite (M) at 7% lattice strain, as schematically expressed by the blue curve in (ii). This provides a much closer match to the expected uniform elastic strain of the nanowire (the red curve). In a composite, at the interface between the nanowire and the matrix, the two bodies share a common strain, as expressed by the green dashed curve. It is obvious that by this concept the elastic strain in the nanowires (or the common strain) also exhibits a spacial distribution corresponding to that of the A-M structure in the matrix. Continued global deformation to 7% will see a complete match between the fully martensitic matrix and the elastically stretched nanowire, as expressed in (iii).

Therefore, in essence this is a martensitic phase transformation assisted "lattice strain matching" concept, between the uniform large elastic strains of nanowires and the uniform lattice distortion strain of the martensitic transformation, and the composite can be considered a "phase transforming matrix composite".

3. Demonstration of the Concept

Using this concept, we designed a NiTi matrix-Nb nanowire in-situ composite.[17] By this principle, various shape memory alloy - nanoinclusion material combinations are possible. There are good range of shape memory alloys, such as Cu-Al-Ni, Cu-Zn-Al, Cu-Al-Mn, Fe-Mn-Al-Ni etc. The primary concerns of selecting the suitable shape memory alloy include high workability to withstand severe plastic deformation, transformation strain, and metallurgical compatibility with the non-inclusion material to be embedded. NiTi was chosen for its excellent

satisfaction of all these criteria. In this work we have also tested CuZnAl and NiTiCu as the matrix alloy with the intention to alter the magnitude of the martensitic transformation strain to be higher or lower than the elastic stain limit of the nanoinclusions. Nb was used as a test material for the nanowire inclusion. It was chosen for its convenience of forming a pseudo-binary eutectic with NiTi, thus allowing the creation of an in-situ composite, and its good workability, so to be easily converted from eutectic lamellae form into nanowires by severe deformation via wire drawing. Other NiTi-X pseudo-binary eutectic systems also exist, such as NiTi-V, NiTi-Ta, NiTi-TiCu, NiTi-Nb_3Sn, NiTi-Ti_3Sn, NiTi-Ti_5Sn_3 and NiTi-Ti_5Si_3.

The NiTi-Nb composite was produced by pseudo-binary eutectic casting of NiTi-Nb system followed by ingot forging and wire drawing to convert the Nb lamellae into nanowires. **Figure 2**(a) shows the composite wire material produced in bulk form. The Nb nanowires are 30~60 nm in diameter (Figure 2(b)), in large aspect ratios (well above 100:1), and all well-aligned along the composite wire direction (Figure 2(c)). The Nb nanowires are practically all single crystalline with exclusive [110] fibre texture along the composite wire direction. The volume fraction of the Nb nanowires is approximately 25%. The NiTi matrix is nanocrystalline.

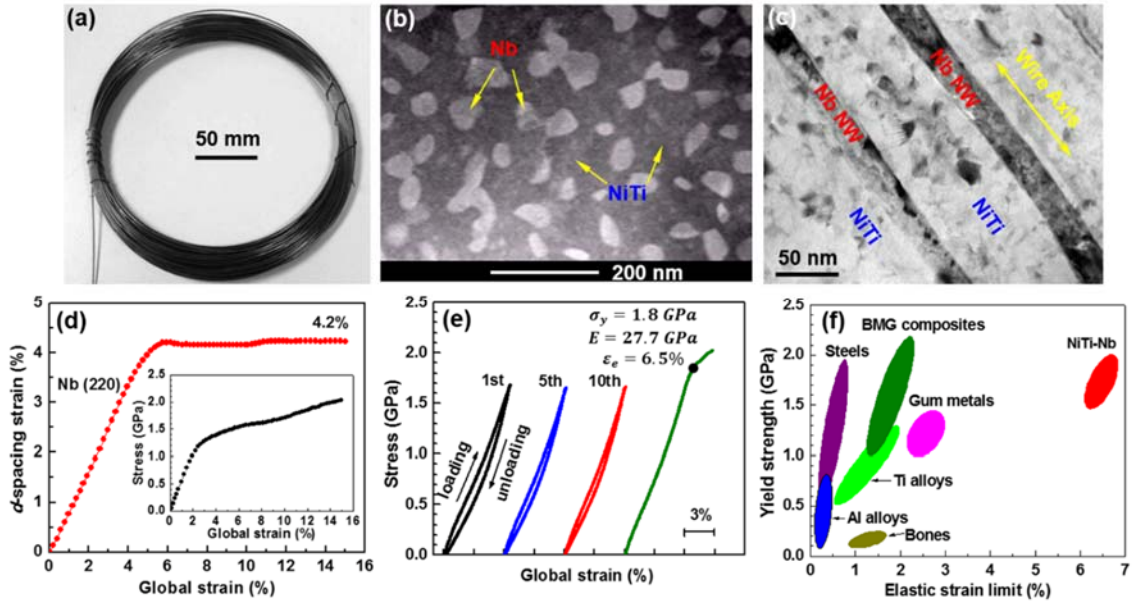

Figure 2. A NiTi matrix–Nb nanowire in-situ composite designed based on the principle of "lattice strain matching".[17] (a) The nanowire composite wire material fabricated by casting, forging and wire drawing. (b) A scanning transmisison electron microscopic image of the cross section of the composite wire. (c) A transmisison electron micoscopic image of the longditudinal view of the composite wire. (d) Nb (220) *d*-spacing lattice strain of the Nb nanowires in the composite wire direction as a functional of the applied tensile global strain. The inset shows its corresponding global stress-strain curve. (e) Tensile stress-strain curves of the composite. These curves were recorded after an initial tension to 9.5% strain. (f) Comparion of yield strengths and elastic strain limits between this NiTi-Nb nanowire composite and other materials. (For reference to the competitor materials shown in Fig. 2(f), please refer to the original publication in [17].) Reproduced with permission.[17] Copyright 2013, The American Association for the Advancement of Science.

Figure 2(d) shows the evolution of the Nb (220) *d*-spacing strain along the composite wire direction as measured by means of in-situ synchrotron high-energy x-ray diffraction (HE-XRD) during tensile deformation. The inset shows the global stress-stain curve of the sample. The Nb nanowires exhibited ultra-large elastic strains of 4.2%. This corresponds to a load bearing of

4.2 GPa by the nanowires in the composite, or a strength contribution of 1.05 GPa to the composite wire sample. Figure 2(e) shows the tensile deformation behaviour of the composite wire after an initial deformation training to 9.5%. The composite exhibited complete superelasticity up to 1.7 GPa stress and 6.5% global strain. It also recoded a yield strength of 1.8 GPa and an apparent Young's modulus of 27.7 GPa.

These properties put the composite in an unchallenged position in the materials mechanical property chart, as shown in Figure 2(f). Its yield strength is comparable to the best engineering metallic materials, but its macroscopic elasticity is more than twice of all other competitor materials. More importantly, this work was the first achievement of such ultra-large elastic lattice strains close to the theoretical limit in bulk form, overcoming a long standing challenge of transcribing the exceptional capabilities of nanomaterials in bulk materials. This achievement was regarded in a special editorial commentary of *Science*[18] to "*herald(s) an era of new possibilities in materials design*". More specifically, the significance of this work can be stated as:

(1) It overcomes a long-standing challenge known as the "valley of death" to transcribe the exceptional mechanical properties of nanomaterials to bulk forms, thus opens an unprecedented opportunity to design and develop practical materials of extraordinary mechanical properties.

(2) It is known that many functional properties of solids, such as photonic, electronic, magnetic, superconducting, photocatalytic and chemical sensing properties, are sensitively related to the interatomic bonding in solids, which can be influenced by elastic strains. The attempt to improve the physical and chemical properties of solids by inducing large elastic strains is an emerging frontier research in materials science, known as the "elastic strain engineering".[11,19,20] This ability to achieve ultra-large elastic strains of solids in bulk forms provides a new and unique possibility for the design and production of "elastic strain engineered" functional materials.

With this in mind, the work has progressed into further areas in the past 6 years, including clarification of the fundamental science of the principle, expansion of the material design scope into other systems, and exploration of elastic strain engineering for material functional properties.

4. Proof of the Concept

This principle of martensitic transformation assisted large lattice strain matching is a new concept in our physical metallurgy literature. Direct experimental evidence is needed to verify the concept and deepen our understanding beyond the logical hypothesis and circumstantial support presented above. To verify this hypothesis, transmission electron microscopic (TEM) studies and synchrotron HE-XRD studies, both in-situ during tensile deformation, have been conducted. **Figure 3** presents a TEM study of the occurrence of ultra-large elastic lattice strains in the Nb nanowires induced by martensitic transformation in the NiTi matrix.[21] Figure 3(a) shows a miniature tensile sample fabricated by means of focused ion beam milling. The sample is about 1000 nm in length and 300 nm in width, and contains two Nb nanowires oriented along the sample length. The Nb nanowires are approximately 30 nm in diameter and 60 nm apart. Figure 3(a) depicts the situation when the sample was deformed to 3.23% tensile strain inside the microscope. Three martensite plates were formed within the NiTi matrix, marked M1, M2 and M3, as seen in Figure 3(b). High resolution images of the Nb nanowire were taken along the length of the nanowire and *d*-spacing values were determined from these images, as presented in Figure 3(c). The top region is the NiTi matrix, where M1 and M3 are formed. The yellow dashed line represent the boundary between the NiTi matrix and the Nb nanowire. The

white dashed box indicate the region within which high resolution images were taken. The *d*-spacing values were determined from these high resolution TEM images at an interval of seven $(110)_{Nb}$ planes, as indicated in the lower part of the Figure 3(c). Figure 3(d) shows the distribution of the $(110)_{Nb}$ *d*-spacing lattice strain along the nanowire length. The lattice strain shows a clear correspondence to the martensite plates formed in NiTi matrix. The Nb (110) lattice strain is the highest, with a maximum of ~8%, at under the tips of the martensite plates and the lowest at the middle between two martensite plates. This observation provides a direct evidence of the ultra-large elastic strains in one body induced by the martensitic transformation in another.

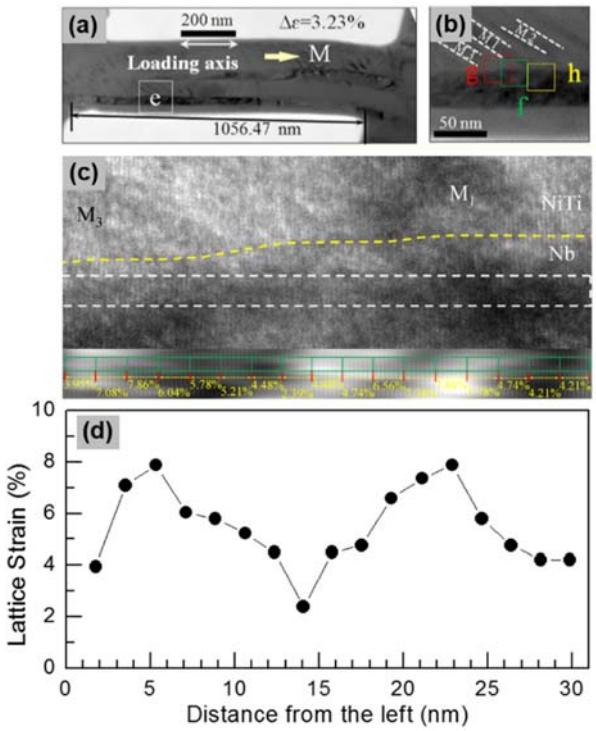

Figure 3. TEM examination of martensitic transformation induced large lattice strains in the Nb nanowires embedded in a NiTi matrix.[21] (a) A miniature plate sample of the NiTi-Nb nanowire composite for in-situ tensile deformation inside TEM, at the moment when deformed to 3.23% tensile strain. (b) Enlarged view of the region marked (e) in (a), revealing the formation of three martensite plates. (c) High resolution TEM image analysis for the determination of the *d*-spacing values. (d) Distribution of the $(110)_{Nb}$ *d*-spacing lattice strain, demonstrating direct correspondence of the ultra-large lattice strains in the Nb nanowire to the martensite plates formed in the NiTi matrix. This work is licensed under a Creative Commons Attribution 4.0 International License.

Figure 4 shows a synchrotron HE-XRD analysis of the correspondence at the macroscopic scale between the lattice strains of the Nb nanowires and the pseudoelastic deformation of the NiTi matrix.[22] Figure 4(a) shows tensile stress-strain curves of the composite, demonstrating the pseudoelastic behaviour associated with the stress induced B2-B19' martensitic transformation in the NiTi matrix. The stress plateaus upon loading and unloading indicate that the deformation (and transformation) proceeded in a macroscopically localized Lüders type manner. Figure 4(b) shows HE-XRD spectrums recorded at one spot within the gauge length section of the sample upon loading during the process of the pseudoelastic deformation. At the moment marked “B” and “C” in (b), the B2-NiTi (211) diffraction disappeared while the B19'-NiTi (001) diffraction appeared abruptly, corresponding to the moment when the B2-B19' martensitic transformation Lüders band front propagated to the XRD observation point. At the

meantime, the *d*-spacing of the Nb (220) planes responded with a sudden jump to a higher value. Similar to the case of loading, the *d*-spacing of the Nb (220) planes showed a sudden jump to a lower value upon the reverse B19'→B2 transformation. Figure 4(c) plots the evolution of the Nb (220) lattice strain during the full pseudoelastic deformation cycle. The sudden increase (B→C) upon loading and decrease (F→G) upon unloading demonstrate the time correspondence of the occurrence of the ultra-large lattice strain in the Nb nanowires to the occurrence of the B2↔B19' martensitic transformation at the XRD observation point.

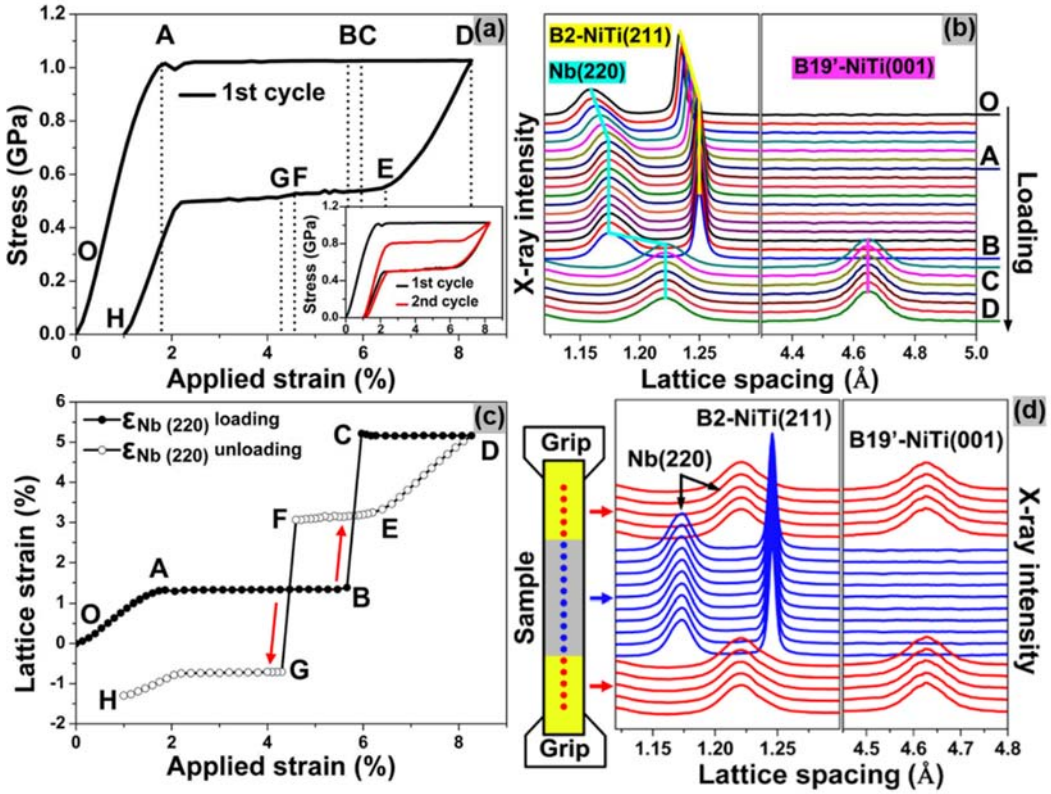

Figure 4. Synchrotron HE-XRD analysis of the correspondence of the ultra-large elastic lattice strains of Nb nanowires to the martensitic phase transformation of NiTi matrix.[22] (a) Tensile stress-strain curves of the composite wire, demonstrating the pseudoelasticity associated with the stress-induced B2-B19' martensitic transformation. (b) Synchrotron high energy XRD spectrums measured during loading of the pseudoelastic deformation cycle in the wire axial direction (the tensile loading direction), revealing the stress induced B2→B19' transformation and the corresponding sudden increase of the Nb (220) *d*-spacing. (c) Evolution of the Nb (220) lattice strain in the wire axial direction during loading and unloading of the pseudoelastic deformation cycle. (d) HE-XRD measurements along the length of the wire sample during the Lüders type deformation, demonstrating the special correspondence of the large elastic strains in Nb nanowires to the B2-B19' martensitic transformation in the NiTi matrix.

Figure 4(d) shows another HE-XRD measurement in the same experiment. In this case the sample was deformed to a given strain corresponding to the middle of the upper stress plateau and held there while XRD measurements were conducted at different locations along the length of the sample, as express by the drawing on the left in Figure 4(d). In this case, the wire sample had certain sections in fully martensitic state within the Lüders bands, as expressed in the yellow coloured sections, whereas the rest remained in B2 austenite state, as expressed by the grey section in the middle. The Nb (220) lattice strain exhibited an ultra-high value of 5.2% in the

section corresponding to the martensite Lüders bands in the NiTi matrix. This gives direct evidence of the uneven Lüders-band type spacial distribution of the elastic lattice strain long the wire length, in confirmation of the concept expressed in Figure 1(b-ii).

5. Other Phase Transforming – Nanoinclusion Composite Systems

5.1. Different Nanoinclusion Morphologies

With the proof of the concept, the design has been trialed in other NiTi-X nanocomposite systems of different nanoinclusion morphologies other than nanowires, including nanoparticles, nanoribbons,[17,23] nanolamellae,[24] and multilayers. **Figure 5** shows an example in a NiTi-Nb nanoribbon composite.[17,23] The composite was fabricated by the same process as for the NiTi-Nb nanowire composite presented above in Figure 2, but with a lower Nb content. Figure 5(a) presents a scanning transmission electron microscopic (STEM) image of the cross section of the composite wire. The composite contained Nb nanoribbons of 5~20 nm in thickness, 50~200 nm in width, and ~12% in volume fraction. Figure 5(b) shows a STEM micrograph of the longitudinal view of the composite wire. The nanoribbons are perfectly aligned along the composite wire and are effectively single crystals with exclusive fiber orientation texture of [110] in the wire axial direction. Figure 5(c) shows a tensile stress-strain curve of the composite wire. The composite reached a tensile stress of 1.88 GPa and an elongation of 18.5%. Correspondingly, the Nb nanoribbons inside the composite reached an elastic lattice strain, based on the Nb (220) *d*-spacing measurement using synchrotron HE-XRD method, of 6.7%, as shown in Figure 5(d). This corresponds to a ~6.8 GPa load bearing in the composite, or ~0.8 GPa contribution to the composite strength. Similar to this nanoribbon composite, other systems have also demonstrated ultra-large elastic strains. For example Nb nanoparticles (~120 nm in size) exhibited 2.0% elastic strains in a NiTi martensitic phase transforming matrix (unpublished work by the authors). In another unpublished work, Nb nanolayers in a NiTi-Nb multilayer nanocomposite exhibited >3% elastic lattice strains.

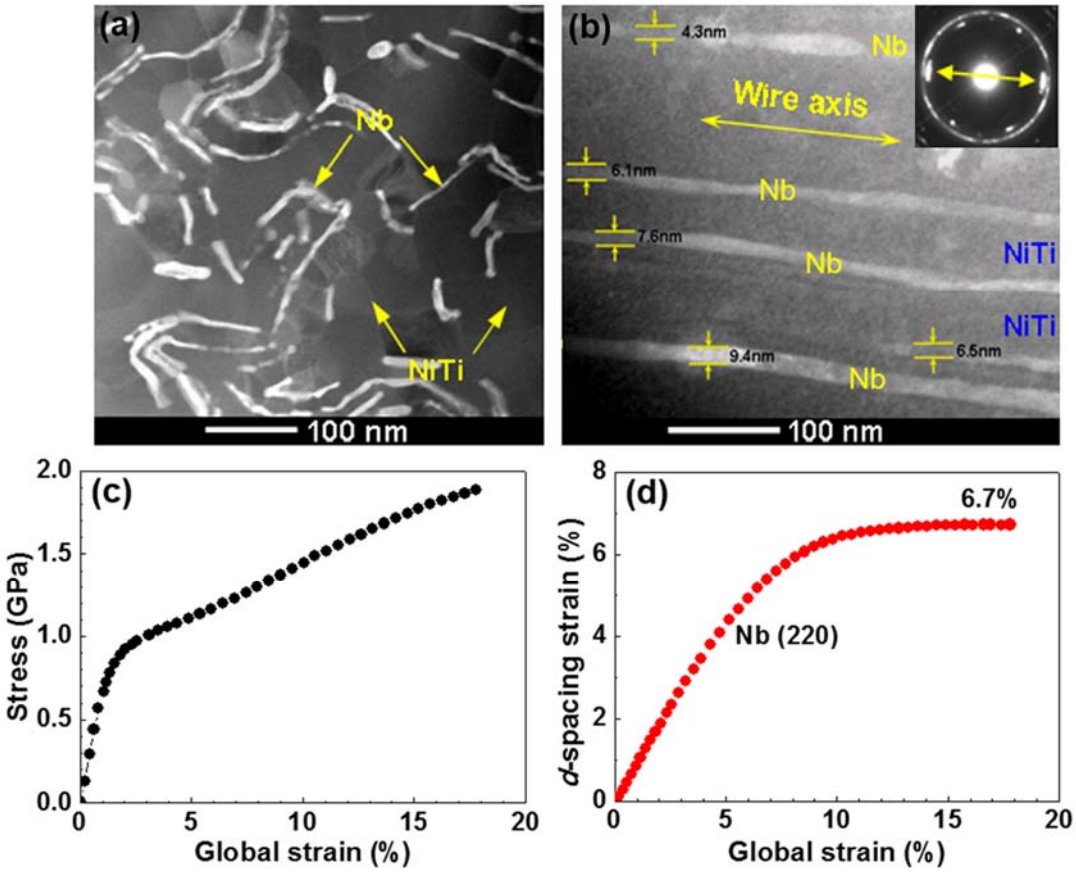

Figure 5. The microstructure and mechanical property of a NiTi-Nb nanoribbon in-situ composite wire.[17] (a) A scanning transmisison electron microscopic image of the cross section of the composite wire. (b) A scanning transmisison electron microscopic image of the longitudinal section of the composite wire, showing perfect alignment of the Nb nanoribbons along the composite wire length direction. The inset shows it corresponding selected-area electron diffraction pattern. (c) A tensile stress-strain curve of the composite wire, reaching a rupture strength of 1.88 GPa and an elongation of 18.5%. (d) Evolution of Nb (220) *d*-spacing lattice strain of the Nb nanoribbons during the tensile deformation, reaching a maximum of 6.7%. Reproduced with permission.[17] Copyright 2013, The American Association for the Advancement of Science.

5.2. Different Nanoinclusion Materials

The work has also expanded to trailing on different materials to form as the nanoinclusions, in particular to test the effectiveness of the lattice strain matching principle in inducing large elastic lattice strains in brittle and rigid materials. These materials, due their generally higher elastic moduli, require higher lattice loads to generate the same lattice strains as for soft materials. This work has included W,[25] Mo,[26] Ti_3Sn,[27] and Ti_5Si_3.[28] **Figure 6** shows a NiTi-Ti_3Sn nanolamellae composite.[27] The composite was produced by a pseudo-binary eutectic solidification between NiTi and Ti_3Sn into a button shaped ingot. Figure 6(a) shows a SEM micrograph of the eutectic microstructure of the composite. The inset is an image of the button ingot fabricated by means of arc smelting. Figure 6(b) is a TEM micrograph of the eutectic microstructure. The Ti_3Sn lamellae are 80~200 nm in thickness and with 200~300 nm spacing in between. Its volume fraction is estimated to be 30%.

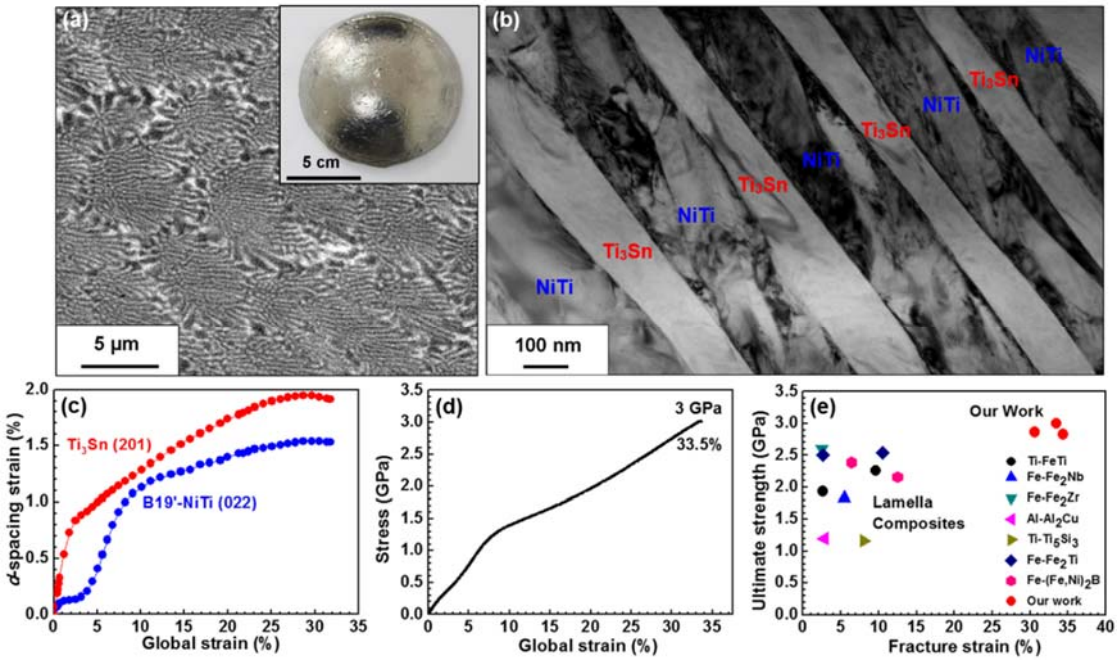

Figure 6. A NiTi-Ti_3Sn nanolamella composite.[27] (a) A scanning electron micrograph of the eutectic microstructure of the composite. The Ti_3Sn phase is in the light contrast. The inset shows the button ingot of the composite fabricated. (b) A transmission electron micrograph of the composite. (c) The evolution of the Ti_3Sn (201) and B19'-NiTi (022) *d*-spacing lattice strain during the deformation. (d) Engineering stress-strain curve of the composite in compression. (e) Comparison of mechanical properties of this NiTi-Ti_3Sn composite with other high-performance metal-based lamella composites in which the soft component is a conventional metal that deforms by dislocation slip. (For the reference to the competitor materials shown in

Fig. 6(e), please refer to the original publication in [27].) This work is licensed under a Creative Commons Attribution-NonCommercial-NoDerivs 4.0 International License.

Figure 6(c) shows the evolution of the Ti_3Sn (201) *d*-spacing lattice strain during compressive deformation. The lattice strain reached a maximum of 1.95%, which is more than six times of what can be achieved in free-standing bulk Ti_3Sn (usually below 0.3%), demonstrating the effectiveness of the stain matching principle on brittle and non-plastically deformable materials. The NiTi-B19' (022) *d*-spacing lattice strain also reached a maximum of 1.5%. It is noted that the lattice strain of Ti_3Sn is higher than that of the NiTi matrix throughout the deformation process. This "extra" lattice elastic stain in Ti_3Sn is obviously caused by the effect of lattice strain matching from the martensitic reorientation in the NiTi matrix. It is evident that the maximum difference in the lattice elastic strains between the two occurred in the initial deformation stage, in which the martensitic reorientation occurred in the NiTi matrix.

Figure 6(d) presents a compressive engineering stress-strain curve of the composite. The composite reached a strength of 3 GPa and a compressive fracture strain of 33.5%. Such properties are superior to practically all competitor metal matrix lamella composites, as presented in Figure 6(e). This is attributed to the lattice strain matching effect of the martensitic reorientation in the NiTi matrix in this composite, which differs from all other comparing composites in which the matrix deforms by conventional plasticity via dislocation slip. The ultra-large elastic strain of the Ti_3Sn component in the composite corresponds to 4.0 GPa load bearing contribution, which translates to approximately 1.2 GPa strength contribution to the composite.

Similar results have also been achieved in other brittle inclusion phases, including 2.9% elastic lattice strain for W nanoribbons,[25] 1.8% for Mo microfibers,[26] and 2.1% for Ti_5Si_3 eutectic lamellae.[28]

6. Attempt of Elastic Strain Engineering

It is also known that ultra-large elastic strains may induce remarkable changes to the physical and chemical functional properties of solids.[11,19,20] Thus, the ability to generate ultra-large elastic lattice strains in solids in bulk forms provides an unprecedented opportunity to explore the possibility to engineer and control the functional properties of solid materials.[11,19,20] Inspired by this concept, we have also started research in the area of "elastic strain engineering".

In this work the first step is to establish the ability to retain large elastic strains after creating them in solids. **Figure 7** shows a work on retaining the large elastic lattice strains generated in the Nb nanoribbons in a NiTi-Nb nanocomposite.[29] This is achieved by using the non-pseudoelastic shape memory effect of the NiTi matrix. Figure 7(a) shows the stress-strain curves of the composite wire deformed in tension. The sample was deformed progressively to different global strains and then unloaded and reloaded again to the next higher stain levels. It is seen that the sample was not pseudoelastic and the deformation was retained after each unloading to zero stress. Figure 7(b) shows the in-situ synchrotron HE-XRD measurement of Nb (110) lattice strain during the deformation. The strains indicated by the arrows correspond to the condition under zero stress after each unloading, i.e. the retained elastic lattice strain in the Nb nanoribbons. Figure 7(c) plots the dependence of the retained elastic strain of the Nb nanoribbons on the global deformation strain of the composite wire. After the last deformation to 8.7%, the sample, which had a retained elastic lattice strain of 2.8%, was heated to induce the reverse transformation of the oriented martensite in the NiTi matrix. This caused a recovery and reversion of the elastic lattice strain in the Nb nanoribbons, from 2.8% in tension to -2.4%

in compression (the NiTi matrix recovered ~5.8% upon the heating). This compressive strain is also shown in the figure (in positive value). Figure 7(d) presents a comparison of the maximum tensile and compressive strains retained in the Nb nanoribbons achieved in this study with those reported in the literature for various materials, all thin films on substrates (no work has achieved ultra-large elastic strains in bulk composites before this work). The retained elastic strains in the Nb nanoribbons achieved in this work are among the highest. This ability to create and retain large elastic strains in solids provides an opportunity to develop better functional materials in bulk forms.

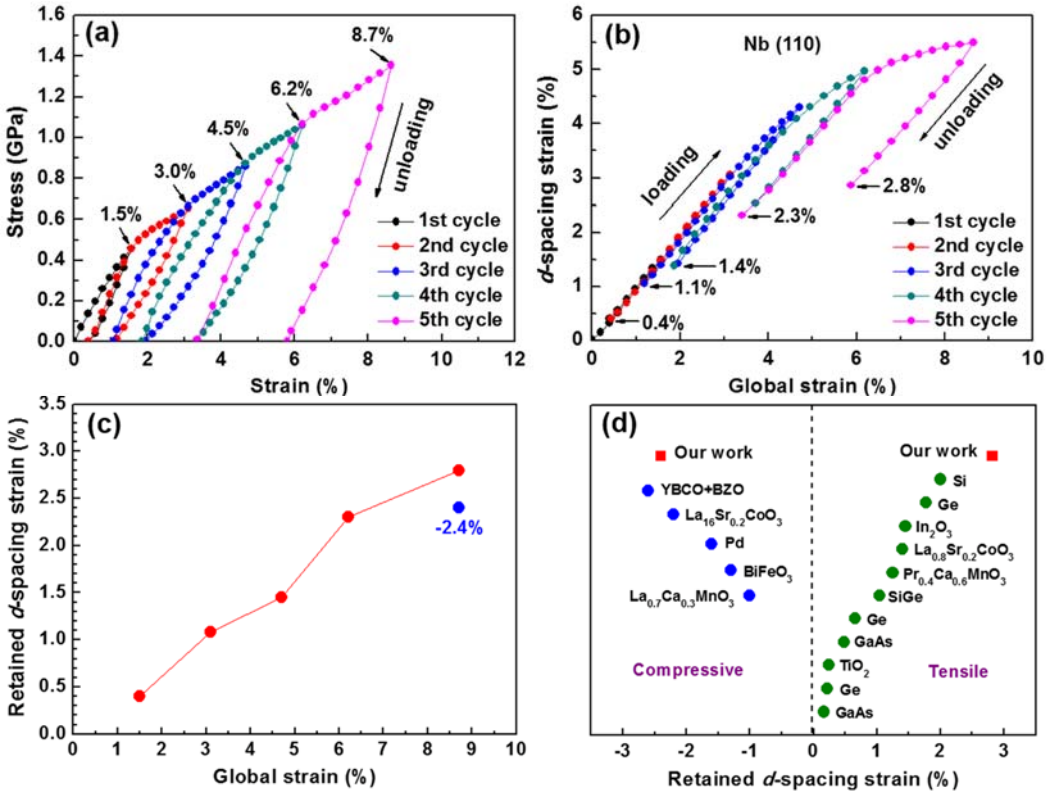

Figure 7. Retention of large elastic strains in the Nb nanoribbons in a NiTi-Nb nanoribbons composite.[29] (a) Progressive tensile loading and unloading stress-strain curves of the composite wire. (b) Nb (110) *d*-spacing lattice strain in the wire axial direction determined from synchrotron HE-XRD measurements. (c) Dependence of the retained Nb (110) *d*-spacing lattice strain after each unloading on the global deformation strain of the composite wire. (d) Comparison of the maximum retained tensile and compressive elastic strains in the Nb nanoribbons in the NiTi-Nb composite with those of thin-film-on-substrate materials reported in the literature. (For the reference to the competitor materials shown in Fig. 7(d), please refer to the original publication in [29].) Reproduced with permission.[29] Copyright 2016, American Chemical Society.

Following the concept of "elastic strain engineering",[11,19,20] we have conducted measurements on the superconductivity of Nb nanoribbons in a NiTi-Nb composite[29] and electrochemical measurements of Pt film on a NiTi substrate.[30] **Figure 8** shows superconductivity measurement of the Nb nanoribbons inside a NiTi-Nb composite.[29] The composite wire samples were pre-deformed in tension to different levels of strains to induce retained elastic lattice strains in the Nb nanoribbons. Figure 8(a) shows the magnetic field-magnetization (H-M) curves at 2 K of the composite wire samples after deformation. The samples magnetized in the opposite direction to the applied magnetic field, demonstrating the typical superconductive response. The minimum on each curve represents the critical magnetic field to reverse the

change of the opposite magnetization of the superconductor, i.e. a coercive filed of superconductivity, denoted H_{c1}. Figure 8(b) shows another measurement of the magnetization behaviour of the Nb nanoribbons in the composite. The samples were cooled under zero field to 2 K, and then a small magnetic field of 10 Oe was applied to induce a negative magnetization due to the superconductive effect. The samples were then heated under this bias field, until superconductive effect was coerced to the normal magnetic response. The T_c indicates the critical temperature for the loss of superconductivity. Figure 8(c) plots the effect of the retained elastic strains on the coercive magnetic field and the critical temperature of superconductivity of the Nb nanoribbons in the composite. It is seen that both the coercive field and the critical temperature increased with increasing the retained elastic lattice strain in the Nb nanoribbons.

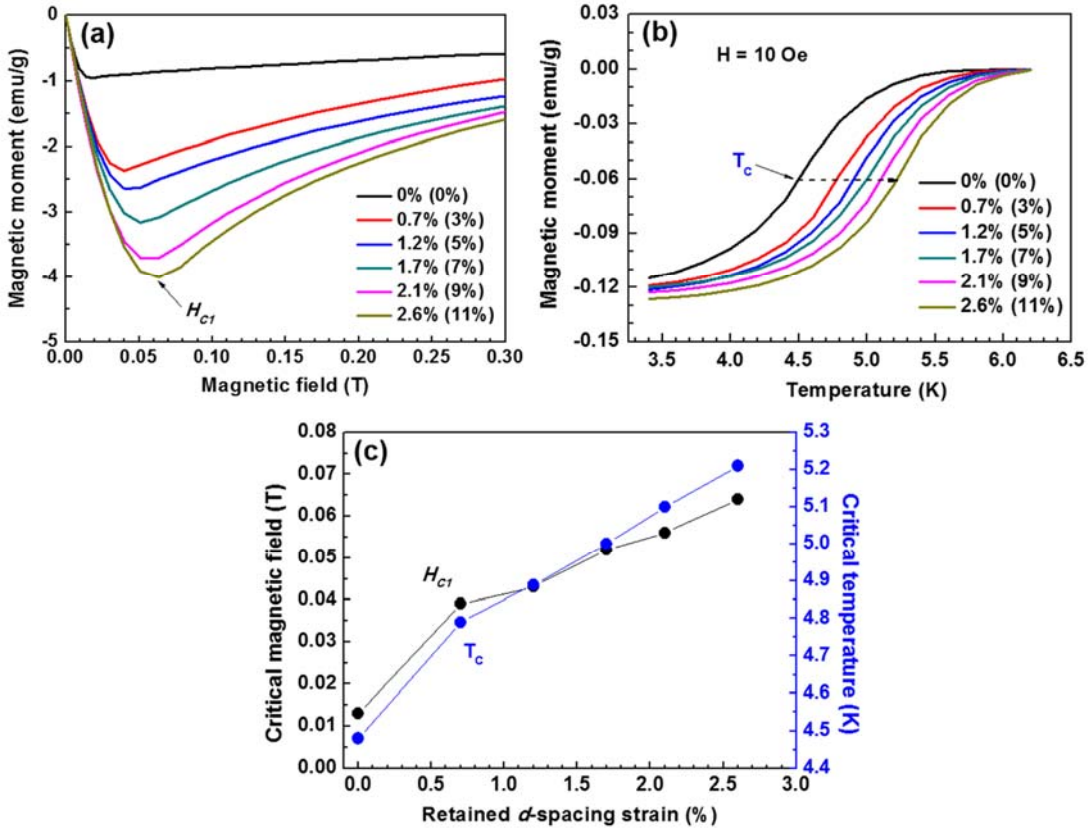

Figure 8. Effect of elastic lattice strain on the superconductivity of the Nb nanoribbons embedded in a NiTi-Nb composite.[29] The samples were pre-deformed in tension to different stains to induce retained elastic lattice stains in the Nb nanoribbons. (a) Magnetisation curves of the samples at 2 K, demonstrating the superconductive response of negative magnetisation of superconductivity of the Nb nanoribbons. (b) Effect of temperature on the reversion of the superconductive magnetisation of the Nb nanoribbons in the composite. (c) Effect of retained elastic lattice strain on the coercive magnetic field and the critical temperature of superconductivity of Nb nanoribbons. Reproduced with permission.[29] Copyright 2016, American Chemical Society.

7. Future Outlook

The progress of the research to date can be described as following:

(1) It has demonstrated the validity of the principle of martensitic transformation assisted lattice strain matching for inducing ultra-large elastic strains in nanoinclusions in bulk composite, by using the unique characteristics of uniform crystallographic lattice distortion of the martensitic transformation in metals.

(2) It has demonstrated the generality of the principle and its applicability to a range of

composite systems of different nanoinclusion morphologies, nanoinclusion material types, and composite forms.

(3) It has demonstrated initial evidence of using this as a possible method to influence the physical and chemical properties of solids, offering new opportunities for "elastic stain engineering".

However, this work is only at the start, and there are potential opportunities for more and greater achievements. In addition, the principle of martensitic transformation assisted lattice strain matching is a new concept, and much is yet to be understood, both in fundamental science and engineering capability. The following may be suggested for future research.

7.1. Fundamental understanding

Whereas the study presented in section 2 has provided the first direct evidences of martensitic transformation assisted lattice stain matching, much more is to be learnt of the actual mechanisms of this phenomenon. For example, each nanoinclusion morphology represents a different mechanics condition, and this has direct influences on the effective load transfer and lattice strain sharing within the system. These questions may include the efficiency and effectiveness of load transfer of the various nanoinclusion morphologies, the maximum size and the maximum volume fraction of the nanoinclusions to allow achievement of ultra-large elastic lattice strains approaching the theoretical limits, the lattice strain profile inside the body of a nanoinclusion, and the effect of the magnitude of the martensite transformation lattice distortion. This requires both experimental work and theoretical simulation and analysis.

7.2. Materials design and optimization

The initial composites designed on this principle was produced through in-situ eutectic solidification. This limits the choice of the matrix and the nanoinclusion materials, and the volume fractions of the two components. Other fabrication approaches need to be investigated and developed, such as the ex-situ multiple layer method used, thin film-on-substrate systems, and multiple-layer thin film systems. Related to the fabrication techniques is the workability of the composites, usually required to convert the inclusion phase into nanoforms. Nanoinclusion morphology optimization is another essential need. This can be guided by the understanding of the fundamental understanding mentioned above.

Materials selection for the matrix and the nanoinclusions is an important factor for achieving superior performances of the composites. Our earlier work was mostly focused on elemental metals, such as Nb, W and Mo, and a few intermetallic compounds, such as Ti_3Sn and Ti_5Si_3. More may be considered, such as alloys and compound, and their metallurgical compatibility with NiTi. Different matrix materials, thus different martensitic transformation systems, can have very different crystallographic lattice distortion types and strains, thus have direct influence on the load transfer and strain sharing between the matrix and the nanoinclusion. These need to be investigated and optimised. This is largely an experimental task.

7.3. Elastic strain engineering

There are examples where large elastic strains cause significant changes to physical and chemical properties of solids. However, many of the known examples are with nano-sized materials, which are impractical for application. This work provides a new opportunity to produce in industrial quantity bulk materials in which ultra-large elastic strains can be induced and retained. For this much guidance is needed from theoretical studies and simulations on the type of materials and types of their functional properties that may be sensitive to elastic strains, so to enable targeted design of martensitic transforming matrix – nanoinclusion composites for

achieving such properties. This will be mostly a theoretical analysis, for example density functional theories analysis and molecular dynamic simulation studies.

These tasks require input of many different expertise, and we welcome and appreciate the opportunity to collaborate with interested scientists.

Acknowledgement

This ongoing research has been supported by a number of research grants. The authors wish to acknowledge the financial support of the National Natural Science Foundation of China in grants No. 51731010, 51601069 and 51571212, the financial support of Australian Research Council in grants DP180101744, DP180101955 and DP190102990. The use of the Advanced Photon Source at Argonne National Laboratory was supported by the US Department of Energy, Office of Science and Office of Basic Energy Science, under Contract No. DE-AC02-06CH11357. We acknowledge the facilities, scientific and technical assistance of the Australian National Fabrication Facility at the Centre for Microscopy, Characterisation & Analysis, The University of Western Australia, a facility funded by the University, the State of Western Australia and the Commonwealth Governments.

References

[1] K. Koziol, J. Vilatela, A. Moisala, M. Motta, P. Cunniff, M. Sennett, *Science* **2007**, 318, 1892.
[2] C. Lee, X. Wei, J. W. Kysar, J. Hone, *Science* **2008**, 321, 385.
[3] E. W. Wong, P. E. Sheehan, C. M. Lieber, *Science* **1997**, 277, 1971.
[4] A. Banerjee, D. Bernoulli, H. Zhang, M. F. Yuen, J. Liu, J. Dong, F. Ding, J. Lu, M. Dao, W. Zhang, Y. Lu, S. Suresh, *Science* **2018**, 360, 300.
[5] Y. Yue, P. Liu, Z. Zhang, X. Han, E. Ma, *Nano lett.* **2011**, 11, 3151.
[6] S. Wang, Y. He, H. Huang, J. Zou, G. J. Auchterlonie, L. Hou, B. Huang, *Nanotechnology* **2013**, 24, 285703.
[7] H. Zhang, J. Tersoff, S. Xu, H. Chen, Q. Zhang, K. Zhang, Y. Yang, C. S. Lee, K. N. Tu, J. Li, Y. Lu, *Sci. Adv.* **2016**, 2, 1501382.
[8] L. Tian, Y. Q. Cheng, Z. W. Shan, J. Li, C. C. Wang, X. D. Han, J. Sun, E. Ma, *Nat. Commun.* **2012**, 3, 609.
[9] G. Richter, K. Hillerich, D. S. Gianola, R. Monig, O. Kraft, C. A. Volkert, *Nano lett.* **2009**, 9, 3048.
[10] J. Frenkel, *Z. Phys.* **1926**, 37, 572.
[11] T. Zhu, J. Li, *Prog. Mater. Sci.* **2010**, 55, 710.
[12] F. Liu, P. M. Ming, J. Li, *Phys. Rev. B* **2007**, 76, 064120.
[13] Y. Dzenis, *Science* **2008**, 319, 419.
[14] P. Podsiadlo, A. K. Kaushik, E. M. Arruda, A. M. Waas, B. S. Shim, J. Xu, H. Nandivada, B. G. Pumplin, J. Lahann, A. Ramamoorthy, N. A. Kotov, *Science* **2007**, 318, 80-83.
[15] L. Thilly, S. Van Petegem, P. O. Renault, F. Lecouturier, V. Vidal, B. Schmitt, H. Van Swygenhoven, *Acta Mater.* **2009**, 57, 3157.
[16] V. Vidal, L. Thilly, S. Van Petegem, U. Stuhr, F. Lecouturier, P. O. Renault, H. Van Swygenhoven, *Scr. Mater.* **2009**, 60, 171.
[17] S. Hao, L. Cui, D. Jiang, X. Han, Y. Ren, J. Jiang, Y. Liu, Z. Liu, S. Mao, Y. Wang, Y. Li, X. Ren, X. Ding, S. Wang, C. Yu, X. Shi, M. Du, F. Yang, Y. Zheng, Z. Zhang, X. Li, D. E. Brown, J. Li, *Science* **2013**, 339, 1191.
[18] M. Zhou, *Science* 339, **2013**, 1161.
[19] J. Li, Z. Shan, E. Ma, *MRS Bulletin.* **2014**, 39, 108.
[20] J. Feng, X. Qian, CW. Huang, J. Li, *Nature Photo.* **2012**, 6, 866-872.

[21] K. Zang, S. Mao, J. Cai, Y. Liu, H. Li, S. Hao, D. Jiang, L. Cui, *Sci. Rep.* **2015**, 5, 17530.
[22] S. Wang, L. Cui, S. Hao, D. Jiang, Y. Liu, Z. Liu, S. Mao, X. Han, Y. Ren, *Sci. Rep.* **2014**, 4, 6753.
[23] L. Cui, D. Jiang, *Acta Metall Sin* **2018**, 55, 45-58.
[24] J. Zhang, S. Hao, D. Jiang, Y. Huan, L. Cui, Y. Liu, H. Yang, Y. Ren, *Acta Mater.* **2017**, 130, 297-309.
[25] F. Guo, S. Hao, X. Jiang, D. Jiang, L. Cui, Y. Ren, *J. Alloy. Compd.* **2019**, 781, 1.
[26] F. Yang, D. Ni, S. Hao, S. Li, Z. Ma, Y. Liu, C. Feng, L. Cui, *Mater. Sci. Eng. A* **2015**, 628, 419-422.
[27] J. Zhang, L. Cui, D. Jiang, Y. Liu, S. Hao, Y. Ren, X. Han, Z. Liu, Y. Wang, C. Yu, Y. Huan, X. Zhao, Y. Zheng, H. Xu, X. Ren, X. Li, *Sci. Rep.* **2015**, 5, 8357.
[28] D. Jiang, S. Hao, J. Zhang, Y. Liu, Y. Ren, L. Cui, *Scr. Mater.* **2014**, 78, 53-56.
[29] S. Hao, L. Cui, H. Wang, D. Jiang, Y. Liu, J. Yan, Y. Ren, X. Han, D. E. Brown, J. Li, *ACS Appl. Mater. Inter.* **2016**, 8, 2917.
[30] M. Du, L. Cui, Y. Cao, A. J. Bard, *J. Am. Chem. Soc.* **2015**, 137, 7397-7403.

Biographies

Yinong Liu obtained his PhD from the University of Western Australia in 1991. He is currently appointed Professor of Materials Engineering at the same university. His research field is physical metallurgy and functional materials, with main interests in shape memory alloys, superalloys, intermetallic composites, magnetic materials, thin films for MEMS applications, and chemical synthesis and functionalities of nanomaterials.

Lishan Cui obtained his PhD from Dalian University of Technology, China in 1994. He is currently appointed Professor of Materials Science and Engineering at the China University of Petroleum (Beijing). His research field is physical metallurgy and functional materials, with main interests in martensitic transformation, shape memory alloys and nanocomposites.

Table of contents

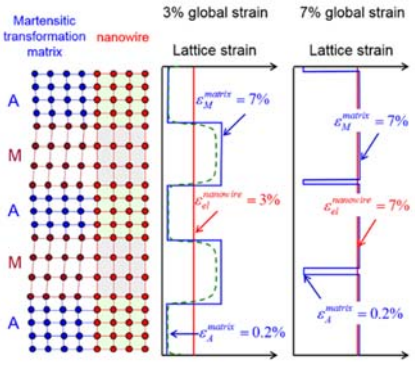

Lattice strain matching between the uniform elastic strains of the nanowires and the uniform lattice distortion strain of the martensitic transformation of the matrix in composites allows effective load transfer from the matrix to the nanowires to induce ultra-large elastic strains in nanowires, overcoming a long-standing challenge to harness the superior intrinsic properties of nanomaterials in bulk forms.